EFFECT OF SECOND PHASE PARTICLE ON FATIGUE CRACK GROWTH BEHAVIOR IN MICROSTRUCTURE CONTROLLED STEELS

(微細組織制御鋼の疲労き裂進展挙動に及ぼす第二相粒子の影響)

BY

MOHAMMAD SUKRI BIN MUSTAPA

(モハマド　スクリ　ビン　ムスタパ)

学籍番号　：　07701589

A DISSERTATION SUBMITTED IN PARTIAL FULFILLMENT OF THE REQUIREMENTS FOR THE DEGREE OF DOCTOR OF ENGINEERING

IN

MATERIALS SCIENCE

DEPARTMENT OF MATERIALS SCIENCE AND ENGINEERING

NAGAOKA UNIVERSITY OF TECHNOLOGY,

NAGAOKA, NIIGATA, JAPAN.

JUNE 2010

Abstract

A series of ΔK-constant fatigue crack growth tests in Paris regime were carried out to investigate the effect of second phase particle on fatigue crack growth behavior of microstructure controlled steels with uniformly distributed hard particles. Three kinds of materials were used in this study, ferrite matrix with pearlite particles (FP), ferrite matrix with bainite particles (FB) and ferrite matrix with martensite particles (FM). The fatigue crack growth tests by using a single edge cracked tension (SECT) type specimen was performed inside a scanning electron microscope chamber equipped with a servo-hydraulic fatigue machine. The results showed that the fatigue crack growth rates for all materials did not coincide with each other, even when the crack growth curves were arranged by the effective stress intensity factor range. From the in-situ observations, crack tip stress shielding phenomena, such as interlocking, branching, etc. were found on the crack wake, which enhanced fatigue crack growth resistance. In ferrite-pearlite (FP) steel, small size and small spacing of hard particles seemed to induce small but frequent crack deflections, which resulted in crack closure phenomena. On the other hand, large size of pearlite particle seemed to induce stress shielding phenomena and then contribute to high crack growth resistance, which was the main reason for higher fatigue crack growth resistance of the large size and spacing of pearlite particle compared to the small size of pearlite particle. It was similar result for the ferrite-bainite (FB) steel where the large size and large spacing of bainite particles enhanced the fatigue crack growth resistance. The higher volume fraction of hard particle also influenced the fatigue crack growth behavior. In this investigation, the result indicated the higher volume fraction of hard particle in the ferrite-bainite (FB1) steel has significantly increased the fatigue crack growth resistance compared to the ferrite-bainite (FB2) with lower volume fraction and ferrite-pearlite (FP) steels. The effect of hardness of second phase

particle was also investigated. The results revealed that the ferrite-martensite (FM) steel showed significantly higher fatigue crack growth resistance compared to the ferrite-pearlite (FP) and ferrite-bainite (FB) steels. From the in-situ observations, the crack tip stress shielding phenomena, such as interlocking, branching, etc were found on the crack wake, which enhanced fatigue crack growth resistance. In the FM steel, the deformation of plastic constrained at the crack tip in ferrite region seemed to induce stress shielding phenomena and then contribute to high crack growth resistance, which was the main reason for lower fatigue crack growth rate of the FM steel with harden martensite particle compared to the FP and FB steels with soften pearlite and bainite particles.

Keywords *: Fatigue crack growth behavior, ΔK-constant fatigue crack growth tests , crack tip stress shielding, interlocking, crack closure, ferrite-pearlite, ferrite-bainite, ferrite-martensite, hard particle, plastic zone size, plastic constrained deformation.*

Table of Contents

List of Figures

List of Tables

Chapter 1 : Introduction

1.1 Introduction of TMCP steel

During the last several decades, steel-making industries have focused their efforts to produce steels with higher toughness, better weldability and less expensive alloying elements. Concurrently, there has been a trend towards the use of higher strength steels to reduce structural weight and fabrication costs. This has been partly possible by introducing a thermo-mechanically controlled process (TMCP). For the TMCP process, the total control during reheating of slab, plate rolling and cooling after plate rolling is important. According to exact definition of TMCP as shown in Fig. 1.1, TMCP includes TMR (Thermo-Mechanical Rolling) and with accelerated cooling (AcC). The aim of TMCP is to obtain the fine and uniform acicular ferrite microstructure instead of ferrite/pearlite banded structure of conventional steels. According to this fine and uniform acicular ferrite, TMCP steels have higher strength and better toughness. The TMCP process is usually to related the AcC. However, the several process variants of the accelerated cooling of plates are shown in Fig. 1.2 [1-3]:-

a) Interrupted Accelerated Cooling: It starts just after the finish of hot rolling and ends at an intermediated temperature, then followed by air cooling. This is the most common case, where plate cooling is generally applied between 800^0C and 500^0C under rates between 5 to 80^0C/s.

b) Direct Quenching: In this case plate cooling is more intense, ending at lower temperatures and generally promoting the formation of a full martensite microstructure. Cooling generally starts at 900^0C and ends at 200^0C, under rates from 5 to 60^0C/s.

c) Direct Quenching Plus Auto-Tempering: This approach of direct quenching uses

plate decalescence (i.e., the surface reheating following accelerated cooling due to the heat flow from its core that is still hot) to promote a direct tempering to the product.

The replacement of a conventional normalizing heat treatment by interrupted accelerated cooling decreased plate grain size from 8-9 ASTM units to 10-11 ASTM units, changing the microstructure from ferrite-pearlitic to a mixture of ferrite, pearlite and bainite. The use of direct quenching decreased even more grain size, to 11-12 ASTM units, and produced a microstructure constituted of bainite, martensite and ferrite [2].

The microstructures of the steels are highly refined as compares to those of conventional processed steels, resulting in a significant improvement in strength and toughness of steels [4-8]. The steels are widely used as structural steels such as in ship structures, pipelines, tanks, buildings, bridges and so on, which require not only strength and toughness but also weldability [9-15]. Steel weldability represents how preferably a steel can be welded without weld defect and how satisfactorily a joint welded with a relevant steel performs during service. In the narrow sense, preferable weldability means that steels can be welded with less hardened heat-affected-zone (HAZ) and without a risk of hydrogen-assisted cold cracking [16, 17]. For concerning the weldability, the caobon equivalent (Pcm) value of TMCP steel is so low that no pre-heating is needed in most cases, as shown in Fig. 1.3. Consequently, TMCP steels have the excellent formability and weldability [18].

1.2 The application of TMCP steel

The typical applications and mechanical strength levels for steel plates produced through TMCP process as shown in Table 1.1. Nowadays about 20% of steel plates rolled all

over the world use this production route; this share doubles in the case of high strength steels, that is, plate with tensile strength over 490 MPa [19].

In shipbuilding, the use of TMCP plates quickly expanded in this field, besides that, it makes feasible the use of high strength steels in this specific application. This product increased the competitiveness of shipyards, as this kind of material allows the reduction of the dimensions of ship components without impairing its performance, decreasing manufacturing and operational costs. The use of accelerated cooling also allows the reduction of carbon and alloy elements contents in steel, increasing significantly weldablility. The use of accelerated cooled plates with yield strength of 315MPa or 355MPa began in 1982; today they represent more than 50% of steel used in a ship. Versions steel more stronger, with 390MPa yield strength, began to be marketed in 1985; nowadays they constitute 30% of steel materials present in a ship. More specifically, 80% of the steel plates used in a ship are processed through TMCP process.

In civil construction, steels especially the 780MPa tensile strength grade are mainly used in the construction of bridges with long spans and high buildings. These steels are produced by TMCP process and in Japan around 10% of these steels are used.

In API pipes, the historical evolution of the alloy design use for API steel pipes along past 40 years as shown in Fig. 1.4 [20]. As can be seen from the figure, the use of controlled rolling with accelerated cooling, allowed a progressive reduction in the carbon content of steel, and simultaneously increased mechanical strength. As a matter of fact, the yield strength of API pipes increased from 360 MPa (API grade X52) to 820MPa (API grade X120) along this time span[1, 2, 8]. This mechanical strength increase allowed reduction of pipe thickness - for example, an API X 120 pipe is 39% thinner than an equivalent API X70 pipe. Thinner pipes are lighter and so transportation is easier and cheaper; the civil works needed for pipe

installation are smaller. Moreover, the area to be welded is also smaller, which contributes to reducing the cost of this expensive process, which is also decreased due to the lower carbon content of the accelerated cooled steel plate. Besides that, the use of accelerated cooling decreases the available time for carbon diffusion during austenitic transformation, reducing the segregation of this element and minimizing the formation of hard constituents which are weak points for hydrogen-induced cracking in pipes that conduct oil with a high H_2S content. So this TMCP process routed plays an effective role for the production of API grade steel plates with higher mechanical strength and hydrogen-induced cracking immunity [1, 2, 8, 21].

Table 1.1: Typical applications of TMCP steel [19]

Application	Tensile Strength [MPa]				
	490	590	690	780	950
Shipbuiding	TMCP				
Offshore platforms	TMCP	TMCP	TMCP		
API pipes	TMCP	TMCP	DQ	DQ	
Civil construction	TMCP	DQ	DQ	DQ	
Bridges	TMCP	DQ	DQ	DQ	
Penstocks	TMCP	DQ	DQ	DQ	DQ
Low temperature tanks	TMCP	DQ			
Cryogenic tanks	TMCP		DQ		
Heavy machines	TMCP	DQ	DQ	DQ	DQ

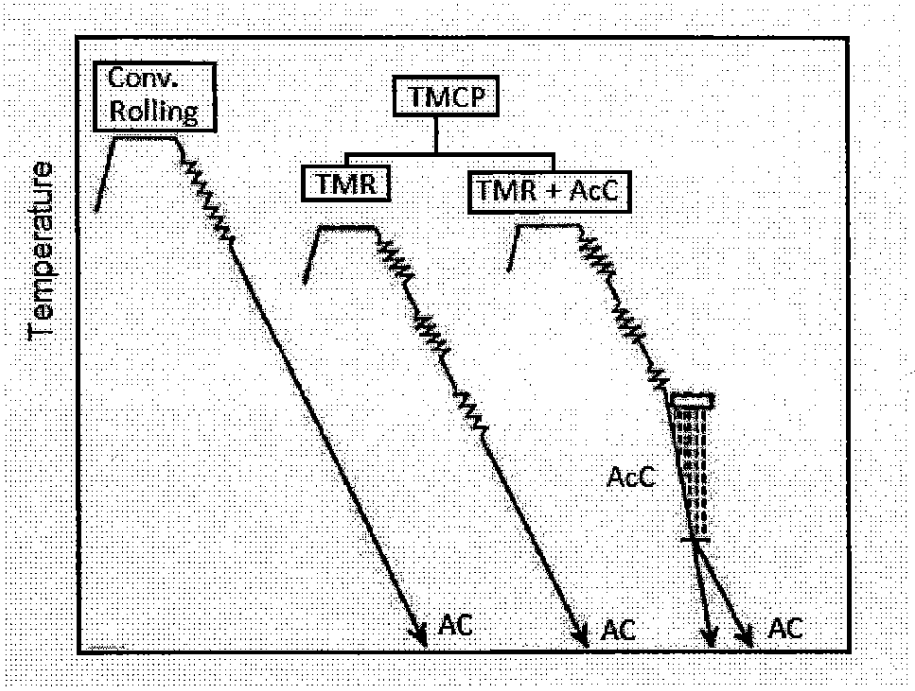

Figure 1.1: Schematic diagram of two method rolling process for conventional and thermo-mechanical control process (TMCP) [2]

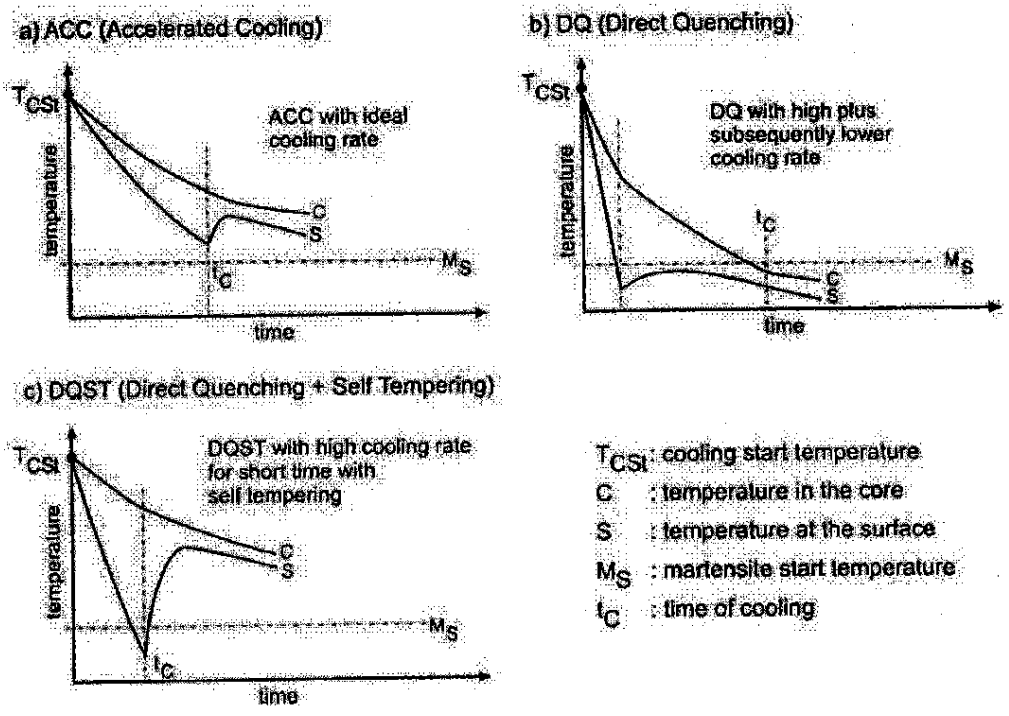

Figure 1.2: Variants of the plate accelerated cooling treatment [2]

1.3 Fracture mechanic approach

It is well known that the presence of cracks threatens the integrity of engineering materials and structures. Under applied load, a crack exceeds to critical size and thereby breaks the cracked member into two or more pieces. This failure mode is known as fracture. Even sub-critical cracks may also propagate to a critical size if crack growth occurs during cyclic (or fatigue) loading. In LEFM, the crack that advances under monotonic, quasi-static loading is characterized by a critical value of the stress intensity parameter denoted by K_C. The critical value of the stress intensity parameter under conditions of small scale yielding and plane strain is generally termed as the fracture toughness, K_{IC}. It has been reported that under cyclic (or fatigue) loading, crack advances from a pre-existing flaw and this phenomenon occurs at stress intensities well below the fracture toughness of the material. Crack growth resulting from cyclic loading is called fatigue crack growth.

When the cyclic stresses applied to a component are small enough, such that the zone of plastic deformation ahead of the advancing is small, LEFM provides appropriate continuum descriptions for fatigue fracture [22]. Paris and Erdogan [23] established the use of LEFM characterization of fatigue crack growth rate based on stress intensity factor range.

$$\Delta K = K_{\max} - K_{\min} \tag{1.1}$$

where, K_{max} and K_{min} are the maximum and minimum stress intensity factor during a fatigue stress cycle, respectively. For an edge-cracked fatigue test specimen,

$$\Delta K = \Delta\sigma\sqrt{\pi a} f\left(\frac{a}{w}\right) \quad , \Delta\sigma = \sigma_{\max} - \sigma_{\min} \tag{1.2}$$

where f is a geometrical factor which depends on the ratio of crack length, a to the width of the specimen W, and σ_{max} and σ_{min} are the maximum and minimum values of a fatigue stress, respectively.

Paris et al. [24] showed that the fatigue crack growth rate (da/dN) is related to the stress intensity factor range (ΔK) by the power law relationship

$$da/dN = C(\Delta K)^m \tag{1.3}$$

where, C and m are experimentally obtained constants and influenced by variables such as material microstructure, environment, temperature, and load ratio, R. The load ratio is defined as:

$$R = \frac{\sigma_{min}}{\sigma_{max}} = \frac{K_{min}}{K_{max}} \tag{1.4}$$

1.4 Fatigue crack growth behavior

Fatigue process can be divided into three stages of crack growth as shown in Fig. 1.5. Region I, is an associated with low growth rates and micro-structurally sensitive growth process. The fatigue fracture process may start from macroscopic cracks that already present in the structural materials during the manufacturing stage. The initiation can start in slip zones adjacent to the outer or at internal voids or inclusions in the materials. Then the mechanism is a process of cumulative plastic strain between slip planes until small crack like defects are produced. Among these initiated cracks, which are greater at a free surface relative to that in the bulk material, only a few may propagate further when the stress concentration is high enough. In this stage the crack propagation is very small (smaller than the lattice spacing) and it is difficult to predict, since it depends on the microstructure of the materials. At the

threshold stress intensity range ΔK_{th} the rate of crack growth is so slow that the crack is often assumed to be dormant or growing at an undetectable rate [25], since the crack driving force is not large enough to overcome the resistance of the crack growth. Sometimes the threshold stress intensity factor is defined as the stress intensity factor at which the crack growth rate, da/dN below than 10^{-08}m/cycles [26-28]. At low ΔK, the low crack driving force leads to a uniform crack front, thereby the crack path becomes more tortuous or irregular, which results in a crack closure effect. The crack closure reduces the driving force in the early contact between the conjugate surfaces during the unloading phase of a load cycles [29-32]. According to Linear Elastic Fracture Mechanic (LEFM) methods, a crack propagation threshold which in a material property exists in this region, below which the crack does not grow.

Above the threshold, there is a significant increase in da/dN with ΔK called Region II. This region also known as the Paris regime is a steady crack propagation phase that is relatively insignificant to microstructure and is characterized by crack propagation normal to the direction of applied loading. In this stage of crack growth has been subjected to many detailed analyses using the linear elastic fracture mechanics [33-37]. At this stage, the stress intensity factor range, ΔK curve is linear and representing the majority of fatigue propagation life. Crack propagation can be quantitatively calculated by using the Paris law. The increment of crack growth with each loading cycle is due to the plastic deformation around the crack tip in many materials. The plastic zone around the crack tip covers many grains at high stress intensity range values. The attendant crack propagates along two slip systems, including the simultaneous or alternating flow. This duplex slip mechanism leads to a planar crack path to the loading axis. It means that fatigue cracks deviate from the primary slip plane and propagate in a direction normal to the maximum principle stress direction.

Finally, dynamic crack propagation may complete the failure process in the stage III. In this stage, the stress intensity factor become equal to the critical stress intensity factor, K_C, where crack growth rates increase rapidly causing catastrophic failure.

1.5 Factors that Influences fatigue crack growth rate

The different mechanisms that affect the fatigue crack growth can be divide into two classes: (a) intrinsic mechanism and (b) extrinsic mechanism, [38] and is illustrated in Fig 1.6. The intrinsic mechanism determines the inherent resistance of a material against fatigue crack propagation. In ductile material, during loading the plastic blunting of the crack tip produces a new fracture surface and unloading reshapes the crack tip and is the dominant intrinsic growth mechanism. However, voids and microcracks in the crack-tip process zone also known as intrinsic effect mechanism. The lower the fatigue crack growth resistance of the material, resulting in accelerated FCG rates. On the others, the extrinsic mechanism causes a reduction of crack tip driving force at the crack tip. They are often referred to shielding mechanism. The most important extrinsic mechanisms are: crack bridging, crack deflection, crack branching and crack interlocking, and crack closure induced by plasticity, roughness and corrosion debris induced closure.

1.6 Crack closure

Premature contact and consequent wedging of the crack faces during the unloading portion of a fatigue cycles at a load above the minimum load is called crack closure [39]. The mechanism has been studied and highlighted by Elber [40] on the basis of experimental observation. Crack closure has been widely accepted as a significant mechanism affecting the crack growth behavior of fatigue cracks, particularly in metallic materials. Elber monitored

the changes in the compliance by using extensometer in thin sheets of cracked 2024-T3 aluminum alloy and argued that a zone of residual tensile deformation is left in the wake of fatigue crack tip. The attendant reduction in crack opening displacement gives rise to premature contact between the faces of the crack and causes a reduction in the apparent 'driving force' for fatigue crack advance. From a continuum viewpoint, it is considered to result from cyclic plasticity which leaves a band of stretched material in the crack wake, a process which is promoted under plain stress condition [39]. The Elber's closure due to residual plastic stretch at crack wake is known as plasticity-induced crack closure (Fig. 1.7(a)). Studies [29, 41] have also revealed other mechanisms of closure which are also active under plane-strain conditions. These mechanisms are illustrated schematically in Fig. 1.7.

The roughness-induced crack closure (RICC) (Fig. 1.7 (b)) is due to contact of rough crack surfaces and was first proposed by Adams [42], Purushothaman and Tien [43], and Walker and Beevers [44]. The RICC occurs when misaligned rough crack surfaces contact during unloading. Rough fatigue cracks have a mixed-mode crack-tip stress state resulting in mode II crack face displacements and asperity misalignment. The resulting contact props the crack open, and reduces the effective crack-tip driving force, ΔK_{eff}. Although RICC is not necessarily restricted to threshold conditions, it is most likely a significant contributor at low ΔK because of the tendency of rough crack paths and smaller crack-tip opening displacement, CTOD. RICC is influenced by (a) small plastic zone size at the crack tip (i.e. typically less than a grain size diameter), which induce single shear mechanism, (b) small CTOD, which are of a size scale comparable to the asperity height such as in the near threshold region, (c) coarse-grained materials with coherent and shareable precipitates capable of inducing coarse planar slip, (d) crack deflection mechanisms and (e) low load ratios where the minimum crack tip opening displacement may be substantially smaller than size of the surface asperities [45].

Oxide induced crack closure (OICC) (Fig.1.7 (c)) was first documented by Walker and Beevers [44], Endo, *et al.* [46], and Suresh, *et al.*[47]. The OICC promotes crack face contact when a voluminous oxide layer forms on the crack surfaces, partially filling the crack mouth. Oxide forms in the crack mouth when freshly exposed surfaces in the crack wake react with environmental agents. Because oxide layers are typically small (approximately 10 Å for aluminum [48]), OICC is negligible where crack-tip opening displacements (CTOD) are large, *i.e.* at high ΔK_{max}. However, OICC becomes dominant in the threshold region as the oxide thickness increases relative to the CTOD [49]. Fretting contact of rough crack surfaces can repeatedly remove portions of the oxide film creating oxide debris in the crack mouth [47]. Oxide debris due to fretting crack surfaces is much thicker than normally expected, resulting in higher crack closure levels.

Crack closure can also be associated with the hydrodynamic action of fluids inside the crack, known as viscous fluid-induced crack closure (Fig. 1.7(e)), and from residual compressive stresses resulting from the dilation associated with an in situ phase transformation, known as transformation-induced crack closure (Fig. 1.7 (d)) [22]. The major types of closure are influenced at low R ratios and stress-intensity level close to the fatigue threshold, where the crack-tip opening displacements are comparable with the dimensions of the oxides or asperity wedges.

Several methods such as compliance technique, potential drop technique, acoustic wave and foil strain gage were introduced for measuring the crack closure [50-57] and compliance technique is the one of the most widely used one. In the compliance technique, during FCG test, crack length was monitored during fatigue crack growth by using compliance data from a back face strain gage. Compliance data from the closure-free portion of the load cycle is used to determine crack length. Load versus strain data (both closure-affected and closure free) can also be used to measure fatigue crack closure event. As the

fatigue crack closes, the effective crack length (a_{eff}) is reduced. The effective crack length is defined here as the crack length measured from the starter notch to the closest point where crack face contact occurs. Schematics of changes in a_{eff} due to crack-tip closure is shown in Fig. 1.8. In Fig. 1.8(a), the entire crack is open and a_{eff} is equal to the actual crack length. During unloading the crack partially closes, so a_{eff} becomes less than the actual crack length, (Fig. 1.8(b)). A strain gage was mounted ahead of the crack tip to detect the crack closing load. The compliance technique (slope of the strain against load curve) has been used to determine the opening load, as shown in Fig. 1.9. From this figure, the steps to determine crack closure as follows; (a) Load-strain loop corresponding to cyclic loading (b) selection of the unloading curve and determination of compliance value and (c) closing load determination.

However, Due to crack closure, the crack can propagate only during fraction of the fatigue loading cycle in which the crack faces are separated. This results in the decrease from the nominal (applied) values of stress intensity factor range, ΔK to an effective stress intensity factor range, ΔK_{eff}.

$$\Delta K_{eff} = K_{max} - K_{cl} \tag{1.5}$$

where, K_{max} is the maximum stress intensity factor and K_{cl} is the stress intensity factor when the cracks opens. Schematic illustration of effective stress intensity factor range under fatigue loading is shown in Fig. 1.10.

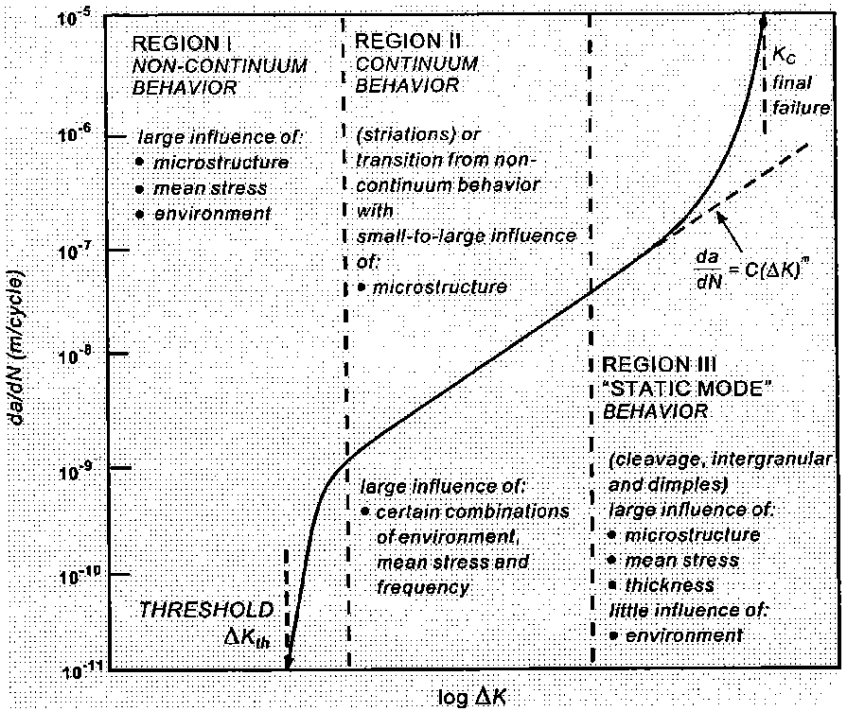

Figure 1.5 : Schematic variation of fatigue crack growth rate, da/dN vs. stress intensity factor range, ΔK [30]

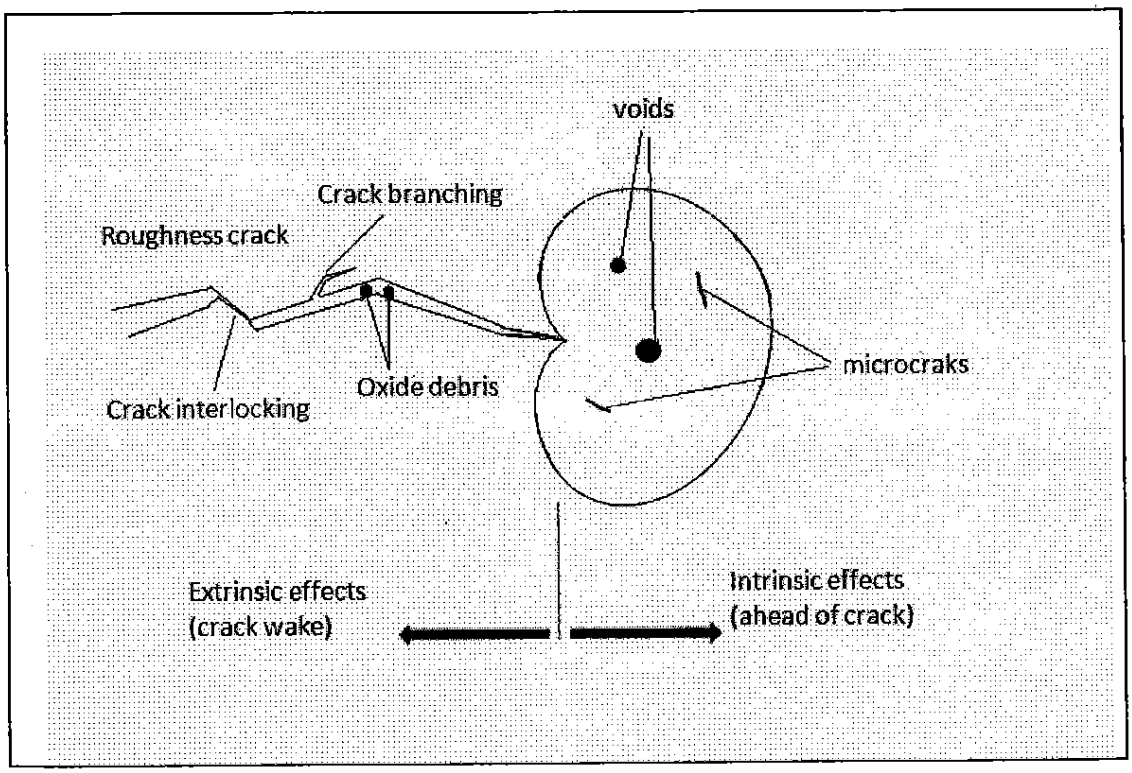

Figure 1.6 : Schematic of illustration of extrinsic and intrinsic effects on FCG behavior

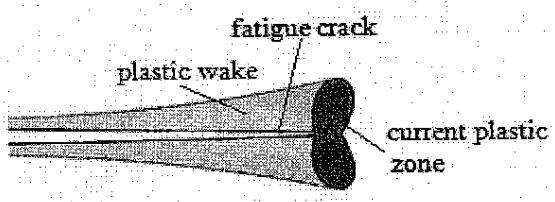

(a) Plasticity-induced crack closure (PICC)

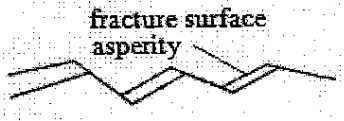

(b) Surface roughness-induced crack closure (RICC)

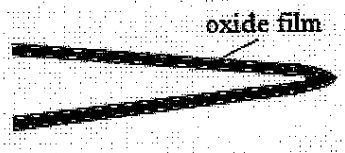

(c) Oxide-induced crack closure (OICC)

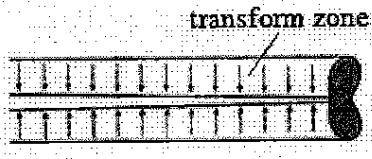

(d) Phase transformation-induced crack closure

(e) Viscous fluid-induced crack closure

Figure 1.7 : Schematic illustration of crack closure mechanisms

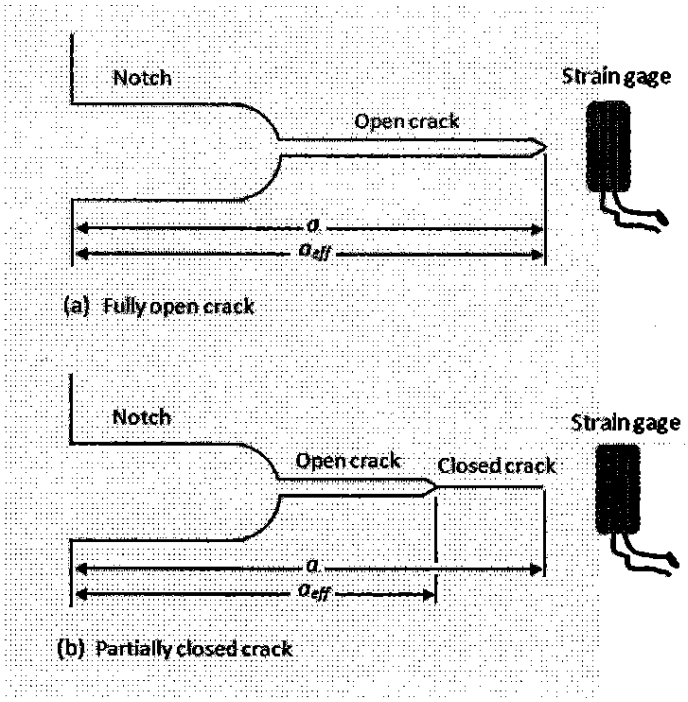

Figure 1.8 : A schematic used to illustrate the effective crack length changed during crack closure.

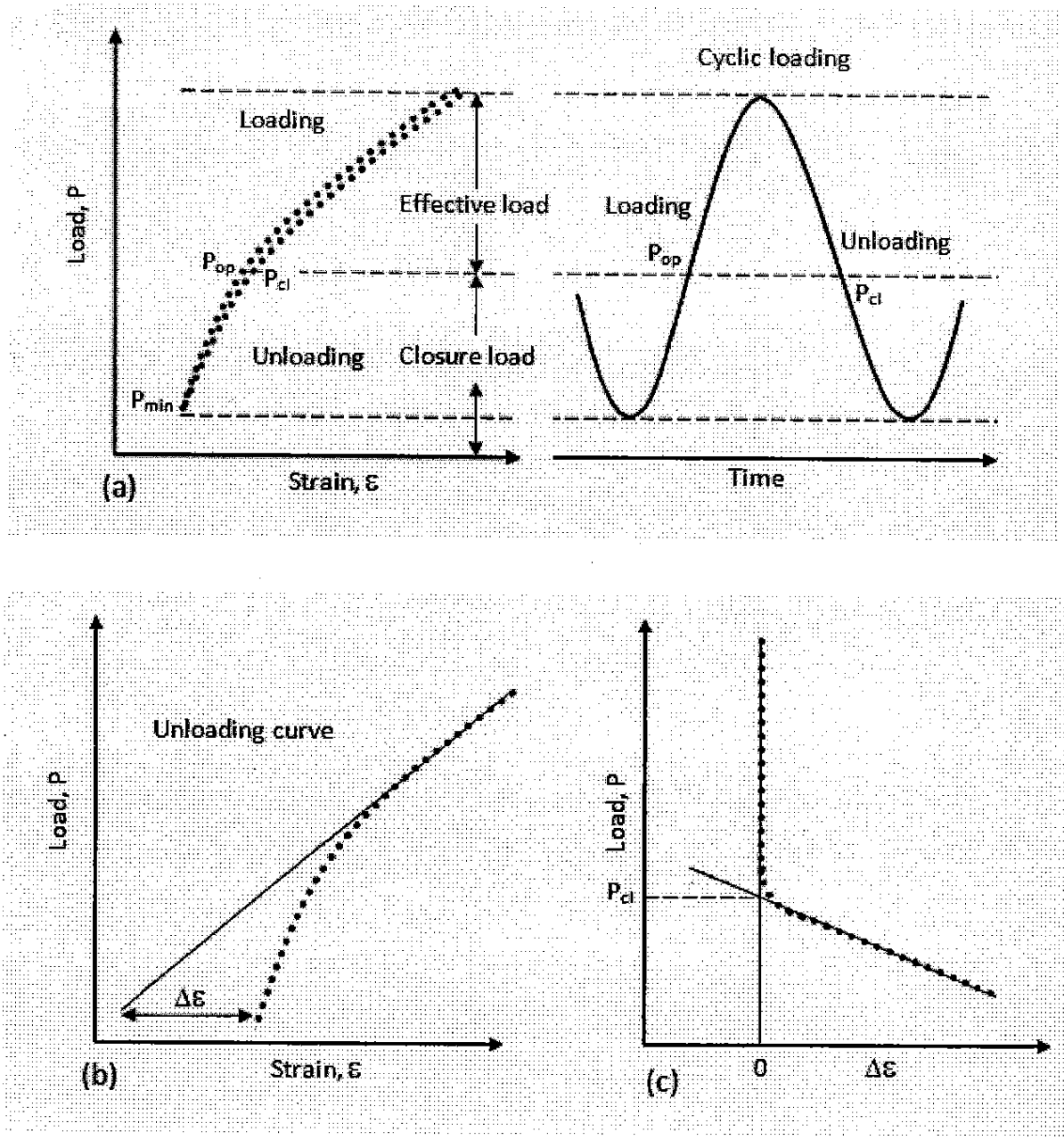

Figure 1.9 : Determination of closing load using the compliance method.

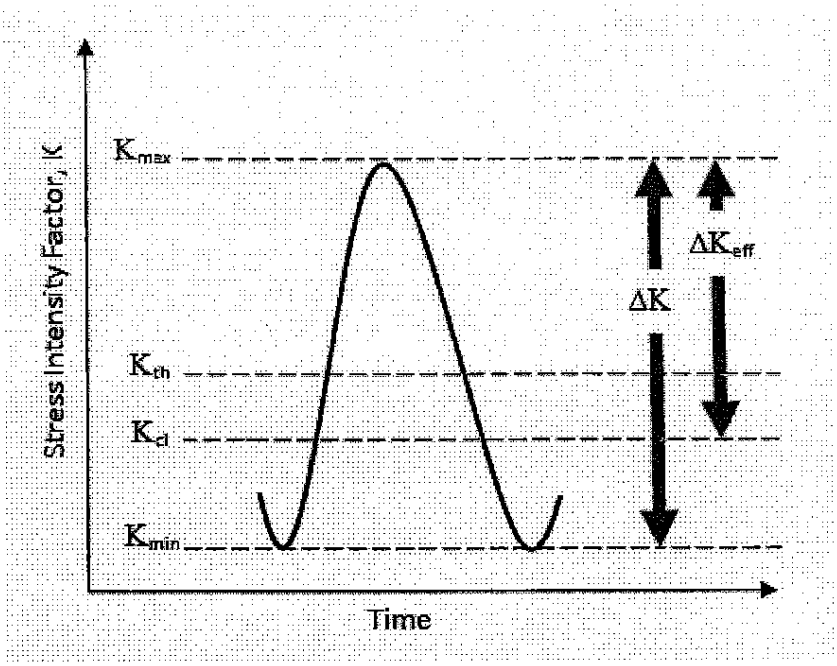

Figure 1.10 : Effective stress intensity factor range, ΔK_{eff}

1.7 Crack tip stress shielding mechanisms

Besides crack closure, crack tip stress shielding another mechanism also affects the fatigue crack growth behavior. Like crack closure, it also reduces the 'driving force' for crack propagation. Therefore, both the crack closure and crack tip shielding are known to be responsible for crack retardation. While the crack closure is widely known and attributed to the crack retardation in metallic materials, the crack shielding is more widely use in non-metallic materials, such as ceramics and composites. In ceramics and composites, the crack tip stress shielding plays a significant role in crack retardation. Fig. 1.11 shows a schematic representation of several crack tip stress shielding.

Under monotonic or cyclic conditions crack tip stress shielding can be expressed as [38]:

$$K_{tip} = K_{\max} - K_s \tag{1.6}$$

$$\Delta K_{tip} = \Delta K - K_s \tag{1.7}$$

where K_{tip} and ΔK_{tip} are the local near tip stress intensity and stress intensity range, respectively, K_{max} is applied or nominal stress intensity, ΔK is the applied nominal stress intensity range given by K_{max} - K_{min}, and K_s is the stress intensity due to shielding.

Crack tip stress shielding has been observed and suggested in crack retardation in ceramics [38, 58-66] and composites [38, 60, 66-72]. In metallic material, crack defection [45, 73-78] and crack branching [79-84] has been observed. It has been reported that crack branching can be introduced due to influence of overloads [74, 79, 80]. However, crack branching would reduce mode I crack driving force and has been known to play a significant role in crack retardation [74, 79, 80, 84, 85].

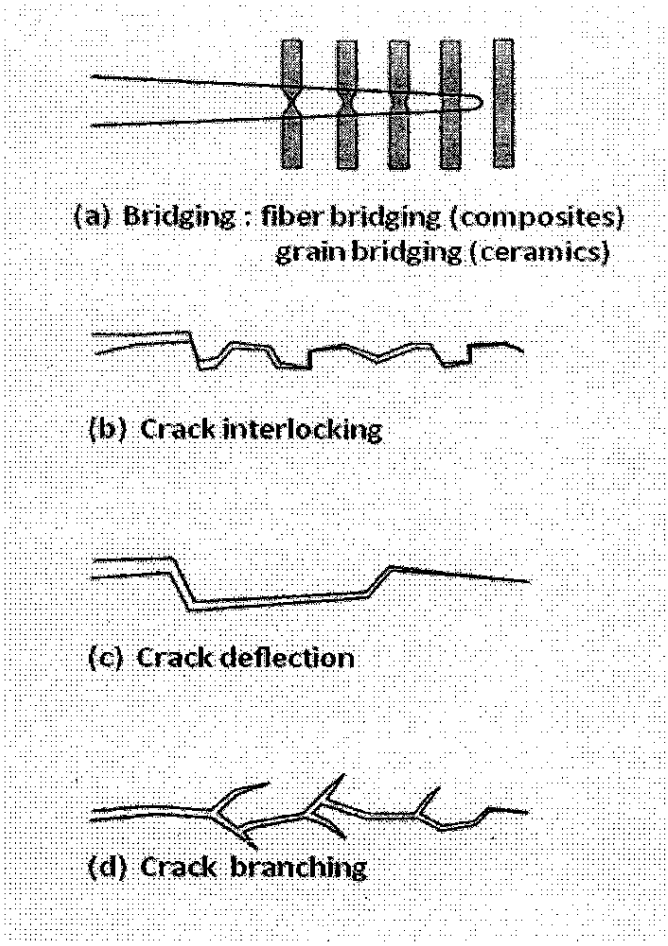

Figure 1.11 : Schematic of several crack tip stress shielding mechanisms

1.8 Literature review

In fatigue crack growth, it is well known that in near-threshold region is largely influenced by micro-structural factors whereas in Paris regime, the microstructures have less influence on fatigue crack growth behavior. Therefore, these regions have received the most attention since they dominate the crack propagation life. There are many microstructural factors that can play a role on fatigue crack growth behavior. Grain size [28, 86], morphology and distribution [73, 87-91], volume fraction [69, 73, 89, 92], hardness [87, 93-95], inclusion [69, 73, 89, 92, 96] and so forth, have important effects on near threshold fatigue crack growth. The effect of grain size on fatigue crack growth behavior has been reported for both near-threshold and Paris regime. In near-threshold regime, coarser grain size has been known to increase the threshold value. While, it was found that grain size appears to have a negligible effect on fatigue crack growth behavior in the intermediate crack growth region [86, 97, 98]. It was also reported that improvement in crack growth resistance with coarser grain size was obtained in the laboratory air [30, 86, 90, 91, 97-103]. Deng et al. [104] have reported that threshold values increase linearly with increasing square root of the grain size. This result from the fact that the larger grain size can lead to higher roughness induce crack closure [105].

Grain size also reported to influence the transition from the near-threshold regime to the intermediate stage (Paris regime) of fatigue crack growth. Experimental observations of such transitions have been reported for titanium alloys [99, 100, 103], aluminum alloys [31, 74, 88, 106, 107], ferrous alloys [30, 101, 105, 108] and nickel-base superalloys [109]. The transition typically occurs when the size of the cyclic plastic zone r_c becomes comparable to the characteristic microstructural dimension l^* of the alloy system.

Related to the study, Suzuki and McEvily [87] carried out the fatigue crack growth tests of dual phase low carbon steels. The materials investigated was AISI 1018 dual phase steel with two different microstructure: (a) martensite with islands of ferrite encapsulated (MEF) and (b) continuous ferrite matrix with islands of martensite encapsulated (FEM). The data showed that MEF steel has higher threshold value (18MPa$\sqrt{m}$) compared to that of FEM microstructure steel (threshold value was 8MPa $\sqrt{m}$). The constraining effect by martensite in MEF microstructure provided higher closure compared to than that in FEM microstructure.

Minakawa and McEvily [73] studied the effect of duplex microstructure on fatigue crack growth in the near threshold region for AISI type 1018, 2.25 Cr-1 Mo, 1045 and 10B35 steels. In steels, threshold level decreases as yield strength increase, a trend followed even for the microstructure of lower ferrite (high carbon) content. Only the low carbon duplex steel showed an exception. In this paper, they reported that, the relationship between crack opening level, K_{op} and stress intensity factor range, ΔK, for low carbon duplex microstructure steel were much higher than those of normalized microstructure at the same stress intensity level. Similar to Suzuki and McEvily results, they also found that the duplex microstructure which consists of a continuous martensite phase encapsulating ferrite indicated high threshold level and yield strength in both the AISI 1018 and 2.25 Cr-1 Mo steels compared to the normalized microstructure due to the high crack closure levels.

Horng and Fine [110] also carried out the similar study of McEvily et al. [73, 87] and showed that the MEF microstructure showed the higher value of threshold and fatigue crack growth resistance in HY80 and 1018 steels. In their research, they also observed the effect of centre notch (CN) and single edge notch (SEN) specimen geometries on near threshold fatigue crack growth behavior. From their observations, it was found that in all cases the SEN

specimens indicated lower fatigue crack growth rate, higher threshold value and crack closure. This is due to high Mode II displacement for SEN specimens, which increase the surface roughness, enhance fretting and crack to close at higher applied stress intensity.

Duta et al. [91] observed the long fatigue crack growth behavior of Fe-2Si-0.1C dual phase steel with ferritic-martensitic microstructures. They reported that the duplex microstructure pronounced fatigue crack growth at load ratio, R (0.05) over wide range from 10^{-8} to 10^{-3} mm per cycle, without changing its strength level. They also reported that microstructure with coarse martensite in continuous ferrite (similar to FEM) and microstructure with fine globular martensite along ferrite boundaries, possesses the highest threshold values, 17.1 MPa $\sqrt{m}$ and 19.5 MPa $\sqrt{m}$, respectively. This is attributed to a meandering crack path, generated by the coarser macrostructure, which promotes roughness induced crack closure and crack deflection effects.

Ramage et al. [94] investigated the effect of phase continuity on fatigue crack growth of a Fe-C-Mn steel with two different microstructures: (a) continuous ferrite (similar to FEM) and (b) continuous martensite (similar to MEF) and reported that the continuous martensite steels exhibited an extremely high fatigue threshold value (20MPa $\sqrt{m}$), compared to continuous ferrite microstructure (threshold value was 16 MPa $\sqrt{m}$). This is due to the higher crack closure in continuous martensite steels, which comes from the high constraint plastic deformation in the ferrite phase.

Shang et al. [69] investigated the effect of volume fraction of martensite of dual phase steel on fatigue crack growth behavior of low carbon steel AISI 1008. The result showed that the volume fraction of martensite was 53% increase the fatigue crack growth resistance. This is due to higher crack closure which was considered to result in a significant contribution to crack tip shielding such as crack deflection and roughness-induced crack closure.

In contrast, Wasynczuk et al.[89] investigated the effects of particle size of ferrite and martensite in a duplex ferrite-martensite microstructured ASIS 1018 steels on fatigue crack growth and reported that the threshold region is not influenced by the volume fraction of martensite.

More recently, Korda et al. [95] was investigated the effect of pearlite morphology on FCG behavior in ferrite-pearlite steel. The results showed that the Steel D (uniformly distributed peralite particle in a ferrite matrix) was lower FCG rate compared to the Steel N (a coarse network pearlite phase with encapsulated ferrite phase). They explained that the higher FCG resistance of Steel D due to the higher crack closure and crack tip stress shielding.

1.9 Significance and objectives of study

In recent years, with the increasing number of aging ships, damage of ship hulls caused by corrosion and fatigue has become a problem. Fatigue damage in ship hull structures are resulted from various type of cyclic loadings including the action of waves, vibration caused by the engine and propellers, and changes in internal pressure due to load. In particular, because the cyclic loadings caused by waves reach an average of roughly 10^8 cycles in 20 years of ship service, these are considered a main factor with a possibility of causing serious accidents in hull structural components [12]. Nippon Kaiji Kyokai [111] lists the intersection between vertical and horizontal members (side longl., trans ring) and the ends of side struts as the category of fatigue members/parts (Fig. 1.12). In 1990s, a lot of fatigue damage occurred at these parts in single-hull very large crude carrier (VLCC) [112]. From a structural viewpoint, it is considerable that these types of damage may also occur in double-hulled VLCC. Moreover, the area around slot openings in double-bottom floor plates is a part where

References

1. Schmidt, D., R. Dehmei, and G. Horn, Latest technologies in plate cooling and their benefit in plate production. Revue de Metallurgie. Cahiers D'Informations Techniques, 2008. 105(5): p. 280-285.
2. Streisselberger, A., V. Schwinn, and R. Hubo. Microalloyed structural plate rolling heat treatment and applications. in Proceedings of the International Symposium Niobium 2001, May 2, 2001 - December 5, 2001. 2001. Orlando, FL, United states: Minerals, Metals and Materials Society.
3. Evans, J.F. and M.T. Clark, Plate cooling - Technologies and market requirements. AISE Steel Technology, 2002. 79(6): p. 49-53.
4. Embury, J.D. and J.L. Duncan, Formability of dual-phase steels. Journal of Metals, 1982. 34(3): p. 24-29.
5. Tamehiro, H., N. Yamada, and H. Matsuda, Effect Of The Thermo-Mechanical Control Process On The Properties Of High-Strength Low Alloy Steel. Transactions of the Iron and Steel Institute of Japan, 1985. 25(1): p. 54-61.
6. Speich, G.R. Physical metallurgy of dual-phase steels. in Fundamentals of Dual-Phase Steels. Proceedings of a Symposium at the 110th AIME Annual Meeting. 1981. Warrendale, Pa, USA: Metall Soc of AIME.
7. Matrosov, M.Y., et al., Use of accelerated cooling to improve the mechanical and processing properties of rolled plates used to make large-diameter gas-line pipe. Metallurgist, 2005. 49(5-6): p. 220-229.
8. Schutz, W., et al., Extended property combinations in thermomechanically control processed steel plates by application of advanced rolling and cooling technology. Ironmaking and Steelmaking, 2001. 28(2): p. 180-184.
9. Tabata, N., et al., Development of thermomechanically control-processed high carbon chromium steels for ball bearing without annealing. 1992, Publ by Kawasaki Steel Corp, Tokyo, Jpn. p. 68-77.
10. Matsuzaki, A., et al. Improvement of mechanical properties of modified 9Cr-1Mo steel by thermo-mechanical control process. in 1990 Pressure Vessels and Piping Conference, Jun 17-21 1990. 1990. Nashville, TN, USA: Publ by ASME, New York, NY, USA.
11. Kusuhara, Y., et al., Structural steel plates for arctic use produced by multipurpose accelerated cooling system. Kawasaki Steel Technical Report, 1985(13): p. 77-82.
12. Igi, S., Y. Inohara, and T. Hirai, High performance steel plates for shipping - Life cycle cost reduction technology of JFE steel. JFE Technical Report, 2005. No.5: p. 13-18.
13. Sekita, T., et al., Materials and technologies for automotives use. JFE Technical Report, 2004. No.2: p. 1-16.
14. Marota, Y., T. Abe, and M. Hashimoto, High performance steel plates for construction and industrial use - New steels plates for contruction and industrial machinery use with high strength and supervior toughness combined with good weldability and formability. JFE Technical Report, 2005. No.5: p. 51-55.

15. Findlay, S.J. and N.D. Harrison, Why aircraft fail. Materials Today, 2002. 5(11): p. 18-25.

16. Yurioka, N., Physical metallurgy of steel weldability. ISIJ International, 2001. 41(6): p. 566-570.

17. Yurioka, N., TMCP steels and their welding. Welding in the World, Le Soudage Dans Le Monde, 1995. 35(6): p. 375-390.

18. Gorni, A.A. and J.H.D. Da Silveira, Accelerated cooling of steel plates: The time has come. Journal of ASTM International, 2008. 5(8).

19. Nishioka, K., Marketing requirements of thermomechanical Processed steel for the 21st century. Steel Word, 2000. 5(1): p. 61-67.

20. Montemarano, T.W., et al., High strength low alloy steels in Naval construction. Journal of Ship Production, 1986. 2(3): p. 145-162.

21. Hillenbrand, H.-G., et al. Manufacturing of X100 pipes for the tap project. in 2006 6th International Pipeline Conference, IPC 2006, September 25, 2006 - September 29, 2006. 2007. Calgary, AB, Canada: American Society of Mechanical Engineers.

22. Suresh, S., Fatigue of materials. 2nd ed. 1998, UK: Cambridge University Press.

23. Paris, P. and F. Erdogan, Critical analysis of crack propagation laws. American Society of Mechanical Engineers -- Transactions -- Journal of Basic Engineering, 1963. 85(4): p. 528-534.

24. Paris, P.C. and F. Erdogon, A critical analysis of crack laws. Journal of Basic Engineering, 1963: p. 528-534.

25. Ritchie, R.O. and J.F. Knott, Mechanisms of fatigue crack growth in low alloy steel. Acta Metallurgica, 1973. 21(5): p. 639-48.

26. Cooke, R.J., et al., The slow fatigue crack growth and threshold behaviour of a medium carbon alloy steel in air and vacuum. Engineering Fracture Mechanics, 1975. 7(1): p. 69-77.

27. McEvily, A.J. and K. Minakawa. On the significance of the threshold for fatigue crack growth. in Advances in Fracture Research (Fracture 84), Proceedings of the 6th International Conference on Fracture (ICF6). 1984. New Delhi, Ind: Pergamon Press, Oxford, Engl.

28. Taylor, D., An analysis of data on fatigue crack propagation thresholds. In Fatigue 84, 1984: p. 327-337.

29. Suresh, S. and R.O. Ritchie, Near-Threshold fatigue crack propagation: A perpective on the role of crack closure. 1985: p. 227-261.

30. Ritchie, R.O., Near-threshold fatigue-crack propagation in steels. International Metals Reviews, 1979. 24(5-6): p. 205-30.

31. McEvily, A.J. and K. Minakawa. Fatigue crack growth in the near-threshold region. in Strength of Metals and Alloys (ICSMA 6). Proceedings of the 6th International Conference, 16-20 Aug. 1982. 1983. Melbourne, Vic., Australia: Pergamon.

32. McEvily, A.J. On crack closure in fatigue crack growth. in Fourth International Conference on Fracture, 19-24 June 1977. 1978. Waterloo, Ont., Canada: Pergamon.

33. Allen, R.J., G.S. Booth, and T. Jutla, Review of fatigue crack growth characterisation by linear elastic fracture mechanics (LEFM). Part II - Advisory documents and applications within national standards. Fatigue and Fracture of Engineering Materials and Structures, 1988. 11(2): p. 71-108.

34. Allen, R.J., G.S. Booth, and T. Jutla, Review of fatigue crack growth characterisation by linear elastic fracture mechanics (LEFM). Part I - Principles and methods od data generation. Fatigue and Fracture of Engineering Materials and Structures, 1988. 11(1): p. 45-69.

35. Lal, D.N., New mechanistic approach to analysing LEFM fatigue crack growth behaviour of metals and alloys. Engineering Fracture Mechanics, 1994. 47(3): p. 379-401.

36. Shields, E.B., T.S. Srivatsan, and J. Padovan, Analytical methods for evaluation of stress intensity factors and fatigue crack growth. Engineering Fracture Mechanics, 1992. 42(1): p. 1-26.

37. Murakami, Y. and S. Nemat-Nasser, Growth and stability of interacting surface flaws of arbitrary shape. 1983. V 17(N 3): p. 193-210.

38. Ritchie, R.O., Mechanisms of fatigue crack propagation in metals, ceramics and composites: Role of crack tip shielding. Papers Presented at the Workshop on the Mechanics and Physics of Crack Growth: Applications to Life Prediction, Aug 4-7 1987, Materials Science & Engineering A: Structural Materials: Properties, Microstructure and Processing, 1988. A103(1): p. 15-28.

39. McEvily, A.J. and R.O. Ritchie, Crack closure and the fatigue-crack propagation threshold as a function of load ratio. Fatigue and Fracture of Engineering Materials & Structures, 1998. 21(7): p. 847-855.

40. Elber, W., Fatigue crack closure under cyclic tension. Engineering Fracture Mechanics, 1970. 2(1): p. 37-45.

41. McEvily, A.J. and K. Minakawa. On the role of crack closure in fatigue crack growth. in Proceedings of ICF International Symposium on Fracture Mechanics (Beijing). 1984. Beijing, China: Science Press, Beijing, China.

42. Adams, N.J., Fatigue Crack Closure at Positive Stresses. Engineering Fracture Mechanics, 1972: p. 543-554.

43. Purushothaman, S. and J.K. Tien, A Fatigue Crack Growth Mechanism for Ductile Materials. Scripta Metallurgica, 1975. 9: p. 923-926.

44. Walker, N. and C.J. Beevers, A Fatigue Crack Closure Mechanism in Titanium. Fatigue of Engineering Materials and Structures, 1979. 1: p. 135-148.

45. Suresh, S., A.K. Vasudevan, and P.E. Bretz, Mechanisms of slow fatigue crack growth in high strength aluminum alloys: role of microstructure and environment. Metallurgical Transactions A (Physical Metallurgy and Materials Science), 1984. 15A(2): p. 369-379.